Journal of Electronic Materials (2024) 53:5926–5936
https://doi.org/10.1007/s11664-024-11152-3

28TH INTERNATIONAL CONFERENCE ON NUCLEAR TRACKS AND RADIATION MEASUREMENTS

Study of Luminescence Behavior in Dy^{3+}-Activated $Ba_3Ca_2(PO_4)_3F$

Shruti Dhale[1] · Nilesh Ugemuge[1] · Vartika S. Singh[2] · S. R. Dhakate[2] · Aniket Bharti[3] · Rajesh Kumar[3] · S. V. Moharil[4]

Received: 16 December 2023 / Accepted: 29 April 2024 / Published online: 23 May 2024

Abstract

$Ba_3Ca_2(PO_4)_3F$, having been proven beneficial for ancient geological surveys, was also found to be an efficient fluorescence emitter when doped with various rare-earth and transition ions. Advancing the respective properties further, dysprosium (Dy^{3+}) was added as an activator into the $Ba_3Ca_2(PO_4)_3F$ host lattice. The Dy ion in its trivalent form possesses emission in two regions, blue at 481 nm and green at 575 nm, opening a new window towards its plausible use in white-light-emitting diode (LED) lighting appliances. Subsequent analyses including x-ray diffraction, Rietveld refinement, photoluminescence, and lifetime observed in milliseconds (ms) revealed a similar nature of the decay curves as given in the literature. Further, a CIE coordinate calculation predicted near-ideal white light emission.

Keywords Luminescence · fluorophosphate · solid-state reaction · CIE coordinates · $Ba_3Ca_2(PO_4)_3F$ (BCPOF)

Introduction

Apatite is a class of naturally existing minerals assigned a hardness of gemstones on the Mohs scale that are too brittle to be used in jewelry. Apatites are typically transparent or translucent but can also be green, blue, violet/pink, yellow, and brown when diluted with transition elements. Early studies include reports on luminescence in apatite systems $M_5(PO_4)_3X$ (with M^{2+} as alkaline earth metals as divalent cation, $(PO_4)^{3-}$ as trivalent anion containing X as F^-, Cl^-, Br^-, or OH^- monovalent anions, categorized as fluorapatite, chlorapatite, bromapatite, and hydroxyapatite, respectively) due to various kinds of impurities.[1–4] The term “apatite” was coined by the mineralogist A.G. Werner in 1788.[5] The word apatite was actually associated with fluorapatites (also written as fluoroapatite), since hydroxylapatites were less known at that time, and chlorapatites were rarely found. Since then, many exciting findings related to emissions involving energy transfer mechanisms using single, double, and more dopants have been observed in these crystals.[6,7] Numerous subsequent studies involving such fluorophosphate-type mineral structures were considered based on a through assessment of their optical properties.[8–19] The presence of a good number of cationic and anionic sites increases the chances of ionic substitutions, making apatite an excellent luminescence host material. The presence of F^- ions endows the compound with greater thermal and chemical stability.[20–23]

In 2015, Zeng et al. reported the practicability of a similar type of compound, $Ba_3GdK(PO_4)_3F$, on doping with Tb^{3+} and Eu^{3+} as rare-earth impurities for white-light-emitting diodes (w-LEDs).[24] $Ba_3Ca_2(PO_4)_3F:Eu^{2+}$ contains broad green emission with an established energy transfer mechanism and observed shifting color coordinates between various activators.[25,26] Very recently, luminescence techniques including photo-, cathode-, and radiation-based luminescence of apatite minerals have been explored for studying rocks, grains, and soil composition for investigating natural disasters that could have happened

---

✉ Nilesh Ugemuge
nileshugemuge@gmail.com

✉ Vartika S. Singh
vartikasingh1710@gmail.com

✉ S. R. Dhakate
dhakate@nplindia.org

[1] Department of Physics, Anand Niketan College, Anandwan, Warora, Dist-Chandrapur 442914, India

[2] Advanced Carbon Products and Metrology, CSIR-National Physical Laboratory, New Delhi 110012, India

[3] University School of Basic and Applied Science, Guru Gobind Singh Indraprastha University, Dwarka, New Delhi 110078, India

[4] Department of Physics, RTM Nagpur University, Nagpur 440033, India

many years ago.[27] Due to the efficient green emission in $Ba_3Ca_2(PO_4)_3F:Eu^{2+}$, photochromism is also seen in the proposed phosphor. Photochromism is an attractive reversible color-changing technique based on exposure to switching light wavelengths. Owing to this remarkable property, associated phosphors can find application in the field of optoelectronics such as photo-switches/sensors, forgery detection, and smart color window shades including sunglasses.[28]

With the growth and advancements in solid-state-based LED lighting technology, the need for more suitable white light sources with high color rendering index ($Ra > 80$) and lower color temperature ($T_c < 7000$ K) for indoor purposes has also increased. Current techniques either involving the coating of yellow phosphor (YAG:Ce) on InGaN chips (emitting blue color) or employing a blend of all three (emitting blue, green, red) phosphors on an ultraviolet (UV) chip in order to realize the actual true color of sunlight have become accepted worldwide. Whereas this involves the use of many phosphor materials with two or three expensive rare-earth materials, the use of single dysprosium (Dy) in its trivalent form can help in lowering the total device cost considerably, since the efficient emission due to Dy^{3+} lies very close to or within the Planckian locus of the CIE coordinate system.[29–37]

With all of the aforementioned points in mind, the present study focuses on the synthesis and the luminescence results for one of the less investigated fluorapatites, $Ba_3Ca_2(PO_4)_3F$ (BCPOF), upon doping with a rare-earth Dy^{3+} impurity, achieving a phase-pure form of this complex host.

Experimental

Synthesis

Synthesis was achieved through high-temperature solid-state reaction. All the initial reactants employed were of analytical reagent (AR) grade. A simple diagram of the entire synthesis process, explained step-by-step, is shown in Fig. 1. First, 1 g barium carbonate ($BaCO_3$), 0.5071 g calcium carbonate ($CaCO_3$), 0.4442 g barium fluoride (BaF_2), and 0.8743 g ammonium dihydrogen phosphate [$(NH_4)(H_2PO_4)$] were mixed together with a mortar and pestle and transferred to a muffle furnace (programmed with a heating rate of 230°C/h) in an alumina crucible, followed by heating at 600°C for 6 h. Further mixing and heating at an elevated temperature of around 1150°C for 8 h and instant quenching thereafter resulted in the successful preparation of the desired complex fluorophosphate

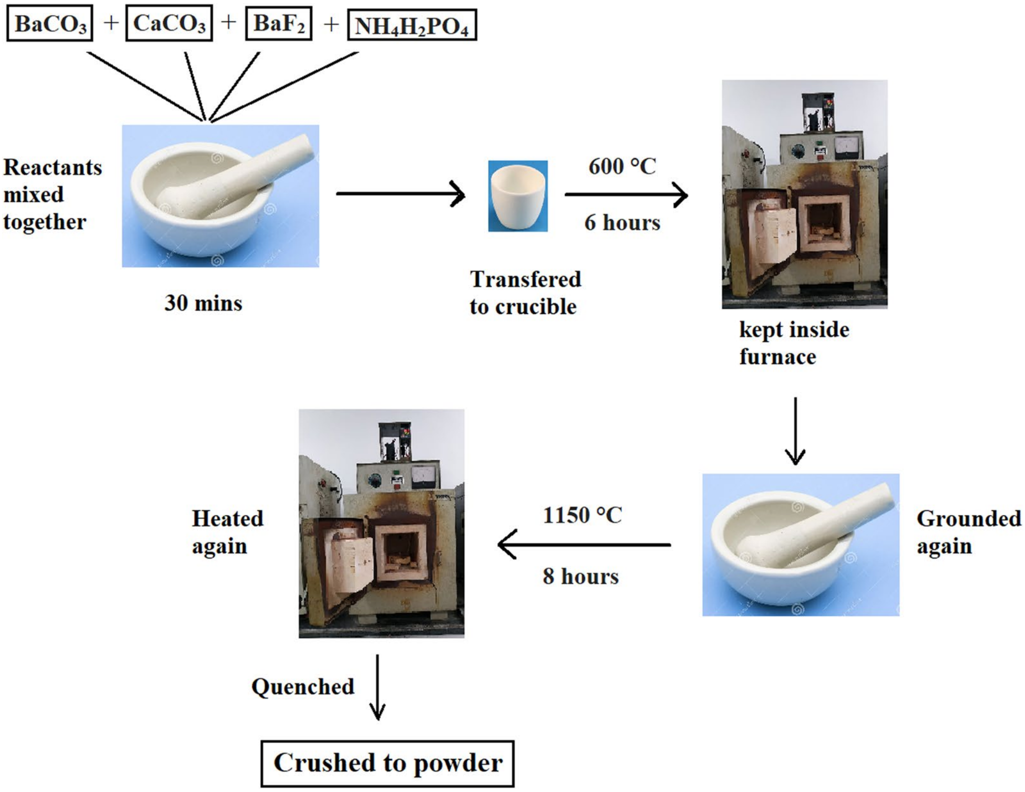

Fig. 1 Synthesis of BCPOF:Dy (x%) ($x = 0.5$%, 1%, 2%, 3%, 5%, 7%) samples by solid-state reaction.

$Ba_3Ca_2(PO_4)_3F$ compound. X-ray diffraction (XRD) studies confirmed the purity of this host compound.

Instrumentation

XRD analyses were performed on a Rigaku MiniFlex II diffractometer. The XRD patterns obtained were refined using the FullProf Suite software program with a least-squares refinement weighting model. Photoluminescence (PL) spectra were obtained using a Hitachi F-7000 spectrofluorometer within the range of 200–700 nm under 5–1 and 1–5 nm slit widths, swapping for emission and excitation recordings, respectively. Photomultiplier tube (PMT) voltage was set at 700 V with a scanning speed of 240 nm/min. Lifetime measurements were also executed on the same instrument, maintaining the scanning time range around 20 ms with a chopping speed of 40 Hz. CIE chromaticity coordinates were obtained using ColorCalculator software (Osram Sylvania, Inc.). All measurements were obtained under room-temperature conditions.

Results and Discussion

X-ray Diffraction (XRD) and Rietveld Analyses

The formation of phase-pure $Ba_3Ca_2(PO_4)_3F$ host material was confirmed in our samples through XRD pattern comparison with standard ICDD 77-0712. Figure 2a displays the XRD comparison between the 2θ lines obtained for our sample $Ba_3Ca_2(PO_4)_3F$ (BCPOF) containing different Dy concentrations in increasing order (0.5%, 1%, 2%, 3%, 5%, 7%), starting from the un-doped pure compound. Figure 2b presents the Rietveld refinement results, with red lines indicating calculated intensities, black crosses as observed intensities, and short green vertical lines showing the position of Bragg reflections of the calculated pattern, whereas the blue lines running horizontally below the XRD patterns indicate the difference between the observed and calculated intensities. The observed values for the goodness-of-fit parameters $R_{wp}=6.2\%$, $R_p=7.4\%$, and $\chi^2=1.063$ are also in good agreement and confirm the quality of our sample. The sample doped with Dy (1%) was considered for Rietveld analysis.

Scherrer Formula and Williamson–Hall Plots

The crystallite size in our proposed phosphor samples was estimated using the Debye–Scherrer equation[38,39] and by drawing W–H plots. The following equations were employed for these calculations:

$$D_{schr} = K\lambda/\beta\,\mathrm{Cos}\theta \tag{1}$$

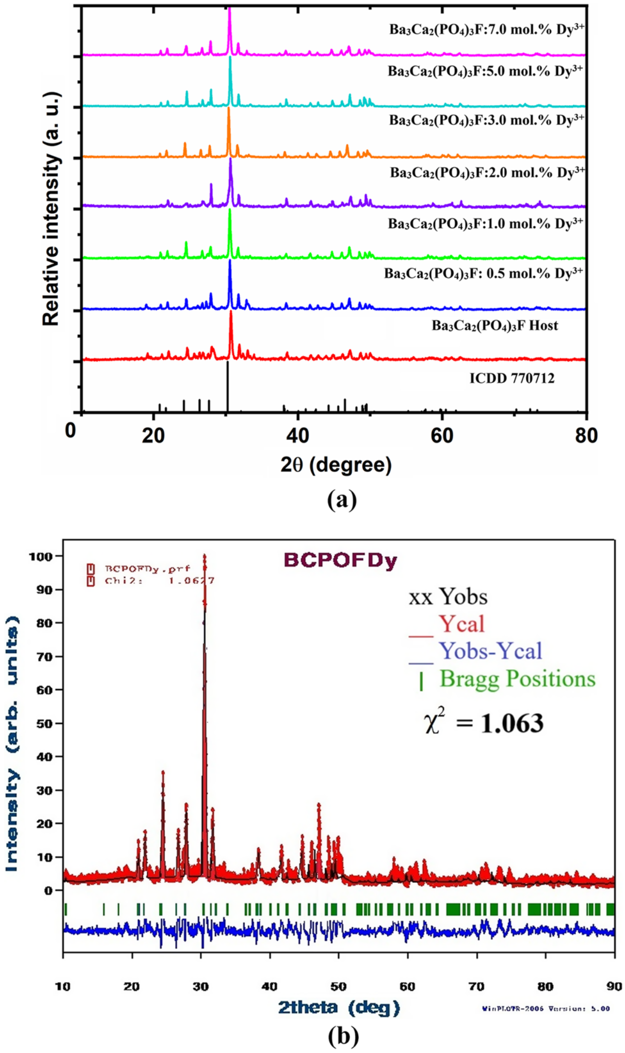

Fig. 2 (a) XRD comparison for all Dy concentrations in the BCPOF host with respect to standard ICDD 77-0712; (b) Rietveld analysis performed on the BCPOF:Dy (1%) sample.

$$\beta\mathrm{Cos}\theta = K\lambda/D_{WHP} + 4(\mathrm{strain})\mathrm{Sin}\theta \tag{2}$$

Equation 1 was used to evaluate the mean crystallite size D_{Schr} for pure BCPOF (host) and doped BCPOF:Dy (1%) samples, using the commonly known Scherrer formula, where K is the Scherrer constant with a value of 0.9, λ is the x-ray wavelength (1.5406 Å), β is the full width at half-maximum (FWHM) of the diffraction peak, and θ denotes the diffraction angle. Similarly, the crystallite sizes in both samples were calculated using the Williamson–Hall equation (Eq. 2), where D_{WHP} represents the crystallite size obtained using W–H plots.[40] Both D_{WHP} and microstrain (ε) depend upon the intercept and slope of the positive straight line obtained from 4 sinθ versus β cosθ graphs.

The various parameters associated with these relations are established and quantified in Table I.

Table I Effective crystallite sizes and strain of $Ba_3Ca_2(PO_4)_3F$ & $Ba_3Ca_2(PO_4)_3F:Dy^{3+}$ (1%) samples

Sample	Effective particle size using W–H plots D (nm)	Standard deviation for D (nm) using W–H plots ($\times 10^{-3}$)	Microstrain using W–H plots ε ($\times 10^{-4}$)	Standard deviation for ε using W–H plots (x 10^{-3})	2θ (degree)	FWHM, β (degree)	Average crystallite size using Scherrer's formula D (nm)
$Ba_3Ca_2(PO_4)_3F$	39.19	2.09	1.415	1.79	30.71	0.264	34.22
$Ba_3Ca_2(PO_4)_3F:Dy^{3+}$(1%)	44.44	0.49	1.655	0.39	30.55	0.249	36.27

The results reveal that the average crystallite size increases upon introduction of the impurity ions inside the host crystal with a decrease in the FWHM (β) degrees from 0.264 to 0.249, and hence confirm the inverse proportionality of the crystallite size versus β.[41,42] The diffraction peaks become narrower upon inclusion of the dopant, resulting in larger particle sizes.[43,44] Therefore, a conclusion can be drawn based on the W–H method that a reduction in β occurs mainly due to the increase in crystallite size.[45] On the other hand, a few studies report an increase in crystallite size only up to a certain higher concentration of the foreign ions, above which it starts to decline. This could be a consequence of quenching that takes place upon the avalanche of the active atoms.[46,47] However, our results show a comparison between the various structurally related quantities evaluated using the obtained XRD patterns of the host and the Dy (1%)-doped samples only. Also, the crystallite sizes calculated using Scherrer's formula are very close to those estimated from the W–H plot diagrams. The level of strain increases as a result of imperfections introduced with the addition of the dopant ions within the lattice.[48] Figure 3 presents the W–H graphs for both the pure and Dy-doped BCPOF samples.

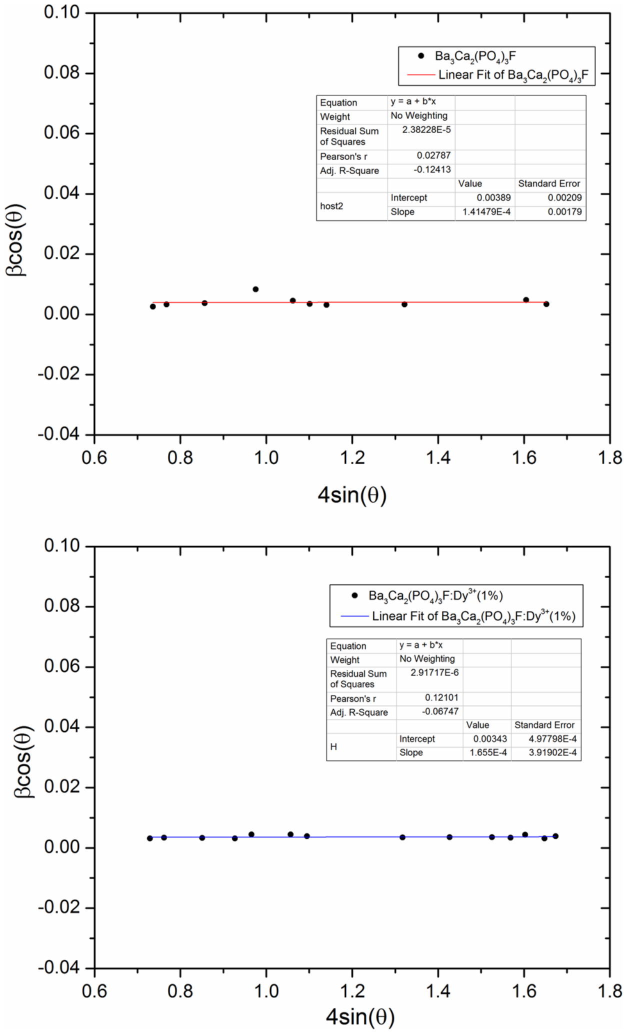

Fig. 3 Williamson–Hall plots drawn for comparison between BCPOF pure host compound and doped BCPOF-Dy (1%) sample.

Photoluminescence (PL) Studies

Dysprosium, one of the versatile rare-earth elements belonging to the lanthanide series, is popular due to its white light emission crucial for w-LED lighting applications. Generally, Dy^{3+} emission consists primarily of two intense peaks, one at 480 nm associated with the $^4F_{9/2} \rightarrow {}^6H_{15/2}$ energy level transition, producing a blue color, and the other at 575 nm emitting a greenish-yellow color that derives from the $^4F_{9/2} \rightarrow {}^6H_{13/2}$ electron transition. Two other emissions at 670 and 757 nm with red and deep-red color are often less intense and difficult to record. Figure 4 shows the PL analysis executed on our Dy^{3+}-doped BCPOF samples. PL emission spectra (Fig. 4a) show two main emissions, with the more prominent one at 480 nm and the second at 575 nm. The white color appears more realistic when the Y/B ratio results in values ≈1. In other words, by adjusting the yellow to blue color peak intensities, it is possible to achieve rich white color emission, which makes dysprosium in its trivalent state (Dy^{3+}) very important for solid-state lighting purposes, assuming greater cost-effectiveness due to the use of a single activator (preferably rare earths) containing phosphors achieving white light combination. Blue emissions are magnetically allowed transitions, whereas a yellow emission is a result of a forbidden electric dipole transition. More accurately, the Y/B ratio determines the site symmetry

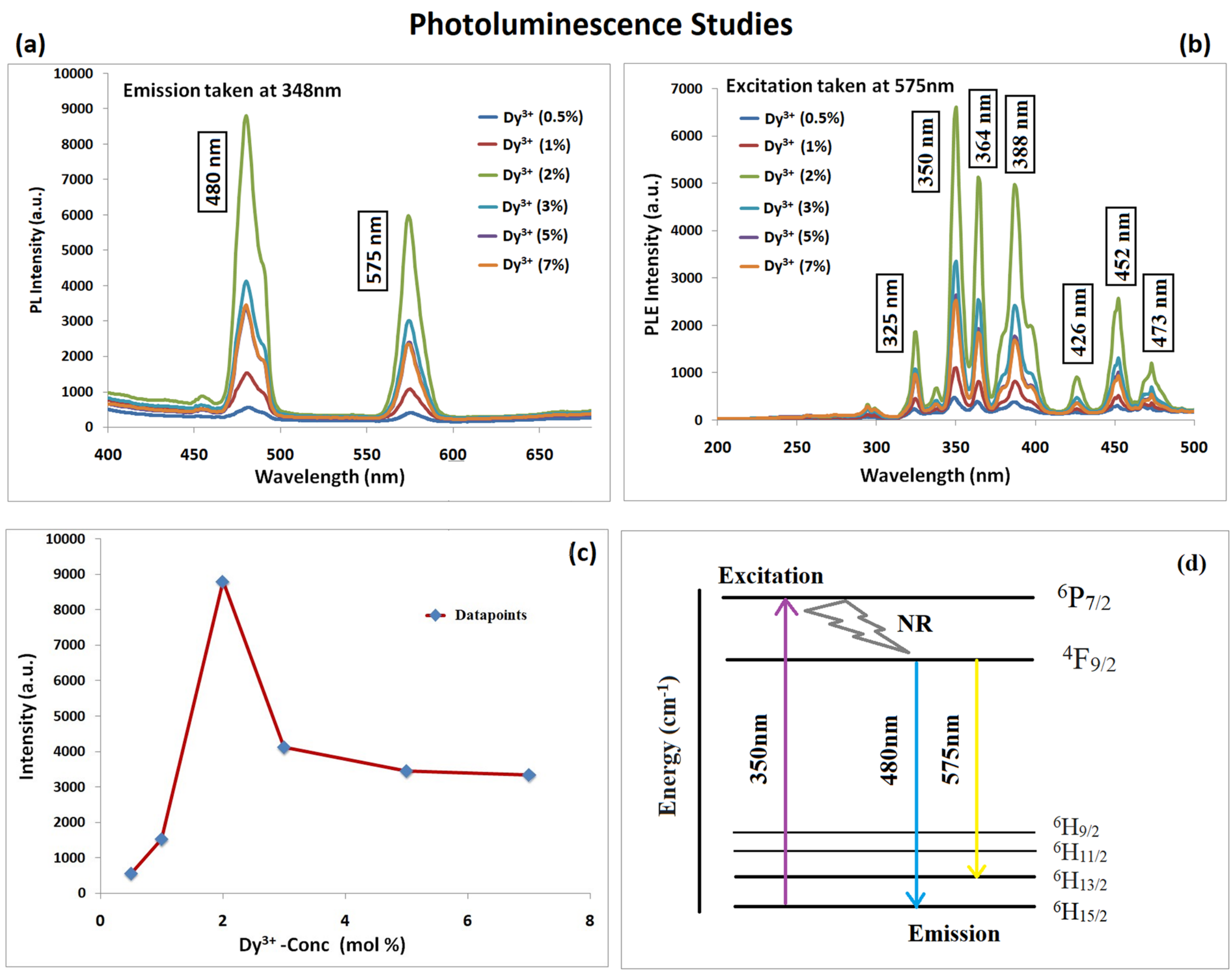

Fig. 4 (a) PL emission spectra taken at 348 nm, (b) excitation recorded at 575 nm emission wavelength, (c) Dy concentration quenching graph showing maximum PL intensity for BCPOF-Dy (2%) sample. Wavelengths are written on the peak intensities for convenience. (d) Energy level diagram of Dy^{3+} in BCPOF host.

Table II Y/B ratio and lifetime kinetics

Dy conc. (%)	Mean lifetime (ms)	Ø%	A (nR) in (s^{-1}) (non-radiative decay rates)	$Y_{(Int)}/B_{(Int)}$ ratio
0.5	0.8755	100	7.2	0.7343
1	0.8452	97	33.7	0.7014
2	0.8140	94	79.1	0.6782
3	0.7912	91	114.5	0.7130
5	0.7624	88	162.2	0.7313
7	0.7240	83	231.8	0.6810

for a Dy^{3+} ion and is considered to be at a higher-symmetry site in the host with inversion centers when the blue emission appears to be more dominant, just like in our case (Fig. 4a).[49–51] The $^4F_{9/2} \rightarrow {}^6H_{13/2}$ transition is more sensitive to a crystalline environment. However, the $^4F_{9/2} \rightarrow {}^6H_{15/2}$ transition associated with blue emission is not significantly affected by the host material, and hence the role of the host crystal on the yellow emission determines the tailoring of output light. Therefore, the ratio of yellow/blue intensities of the dysprosium ions depends upon crystal field effects imposed by the host's structural matrix. Table II depicts the Y/B ratios for our BCPOF samples with different Dy concentrations and suggests the practicability of BCPOF:Dy phosphors in white-light-emitting sources. The PLE spectra shown in Fig. 4b consist of many excitation peaks ranging between 300 nm and 500 nm. The primary and visible spectral lines observed include 295 nm, 325 nm, 350 nm, 364 nm, 388 nm, 426 nm, 452 nm, and 473 nm derived from the transitions of $^6H_{15/2} \rightarrow {}^4D_{7/2}$, $^6H_{15/2} \rightarrow {}^6P_{3/2}$, $^6H_{15/2} \rightarrow {}^6P_{7/2}$, $^6H_{15/2} \rightarrow {}^6P_{5/2}$, $^6H_{15/2} \rightarrow {}^4I_{13/2}$, $^6H_{15/2} \rightarrow {}^4G_{11/2}$, $^6H_{15/2} \rightarrow {}^4I_{15/2}$, and $^6H_{15/2} \rightarrow {}^4F_{9/2}$ electron transitions, respectively. The PL emission and excitation spectra are in accordance with previously reported studies.[40,41] Figure 4c presents a graph of PL intensity versus dopant concentration illustrating the underlying concentration quenching effect when the number of doped ions increases more than a certain value, beyond which the PL intensity starts to decrease. Our proposed sample was optimized for Dy^{3+}(2%) concentration in the BCPOF host. Subsequently, Fig. 4d provides insight into the major electron transitions involved in Dy^{3+} activation.[34,40,52]

Lifetime Decay Kinetics

The observed lifetime decay curves follow first-order exponential behavior (Fig. 5a), and the decay characteristics including quantum efficiency(Ø%), non-radiative decay rate (A_{nR}), and intrinsic lifetime (τ_R) were calculated from the experimentally observed mean lifetime (τ_0) values, using a set of equations described in the literature,[53,54] as summarized in Table II. Shorter lifetime results from closeness to the charge-compensating defects, whereas longer lifetime is seen with greater distance from these defects.[40] In the present case, lifetime is recorded in milliseconds (ms). Figure 5a shows the lifetime measurement decay curves. The

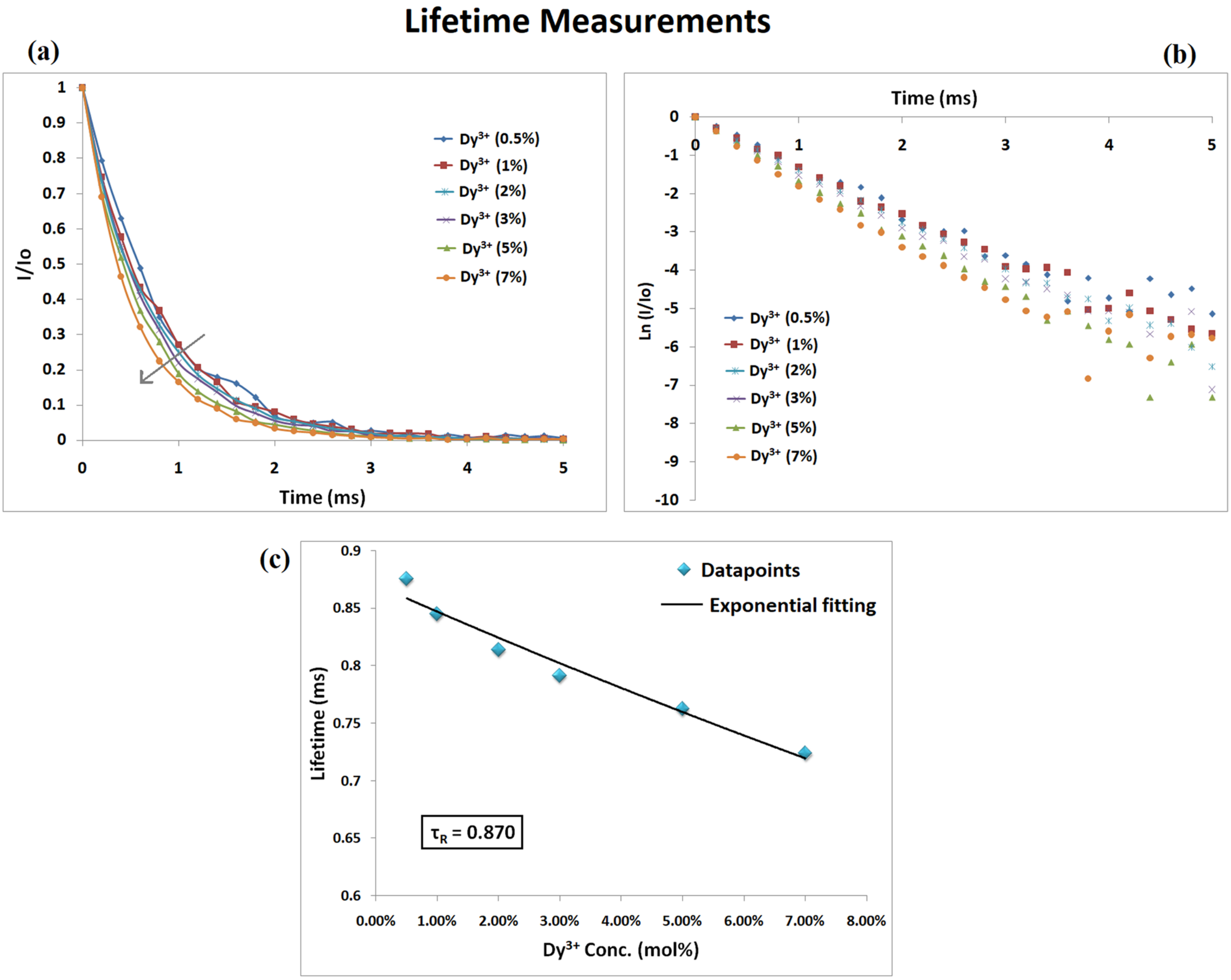

Fig. 5 (**a**) Lifetime decay curves observed for BCPOF samples doped with various Dy^{3+} concentrations, showing an exponential decrease, recorded for 348 nm excitation and 575 nm emission wavelengths. (b) Log(I/Io) versus time (ms) plot displaying a clear picture of the decreasing mean lifetime (τ_0) values with increasing dopant concentrations. (c) Mean lifetime (ms) versus Dy concentration graph, also indicating the exponentially decaying nature of our samples.

direction of the arrow indicates the gradual decrease in lifetime (τ_0) values for the samples with increasing Dy concentration. This occurs because of the greater number of impurity ions in the host crystal, which increases the possibility for non-radiative decay. Therefore, this can be confirmed by the increasing values of the non-radiative decay rates (A_{nR}) given in Table II. Likewise, this is expressed through the log of normalized intensity with respect to the time ordinate graph drawn for all Dy concentrations (Fig. 5b). The experimentally observed lifetime (τ_0) versus Dy concentration graph (Fig. 5c) illustrates the intrinsic radiative lifetime (τ_R).

Crystal Structure Coordination and Dopant Ion Substitution

BCPOF in our sample belongs to the space group $P6_3/m$ (no. 176), and there are two types of divalent cationic sites—M1 (4f) and M2 (6h)—which can be replaced. The two sites carry C_3 and C_{1h} point group symmetries. M1 comprises 9 O^- neighbors at the center with slightly distorted trigonal tri-capped prisms, whereas M2 comprises coordinates 6 O^- and 1 F^- anions. Ba^{2+} and Ca^{2+} can occupy both cationic sites randomly. However, Fig. 6 shows that the actual crystal structure displays Ca^{2+} at M1 and Ba^{2+} at M2. The M1 site is smaller than the M2 site, and hence Ca^{2+} ions are expected to go to the M1 site, so Ba^{2+} finds occupancy at M2. Therefore, the $M1_2M2_3\ (PO_4)_3X$ presents itself as the standard representation formula for the apatite subgroup minerals.[1,8,25]

According to the radius percentage discrepancy equation, the value of D_r dictates the maximum probability for dopant ion substitution. Due to comparable sizes, there is a greater possibility for Dy^{3+} ions to replace Ca^{2+} ions (considering that the ionic radius of Ca^{2+} is 1.06 Å, Ba^{2+} is 1.34 Å, and Dy^{3+} is 1.03 Å).[53]

CIE Color Coordinate System

Selecting Dy-doped phosphors for white-light-emitting sources is the first choice for researchers and industrialists, for many reasons. To achieve the natural quality of colors in artificial light sources, a combination of all three colors—red, blue, and green—is required. Dy^{3+} activates white emission directly by achieving blue and green color together. It is also advantageous to use these phosphors because of their low cost in making devices with an appropriate color rendering index (CRI) and correlated color temperature (CCT).[50,51] CIE color chromaticity coordinates were evaluated, and Fig. 7 shows the position of our optimized sample BCPOF:Dy (2%) on the MacAdam ellipse. We found that the CIE color coordinates observed for our samples lie within the range of the Planckian locus close to the actual white light epicenter with $x = y = 0.3333$ as CIE standard values. CRI values vary from 0 to 100 and measure the deviation from the actual color coordination (deviation from the color that appears in the natural light source, i.e. sun, to the color that appears under the artificial light sources). In other words, it is a kind of measure of color falsity. Color rendering values from 0 to 55 indicate poor, 55–65 fair, 65–75 good, and above 75 excellent results, indicating less color deviation from the original source.

Similarly, color purity quantifies monochromaticity, and for white light emissions, a low value is desirable. Various CIE chromaticity parameters were calculated using the following equations and are summarized in Table III. Higher values of CCT (K) indicate probable use in cool white-emitters.

$$u' = \frac{4x}{12y - 2x + 3} \tag{3}$$

$$v' = \frac{9y}{12y - 2x + 3} \tag{4}$$

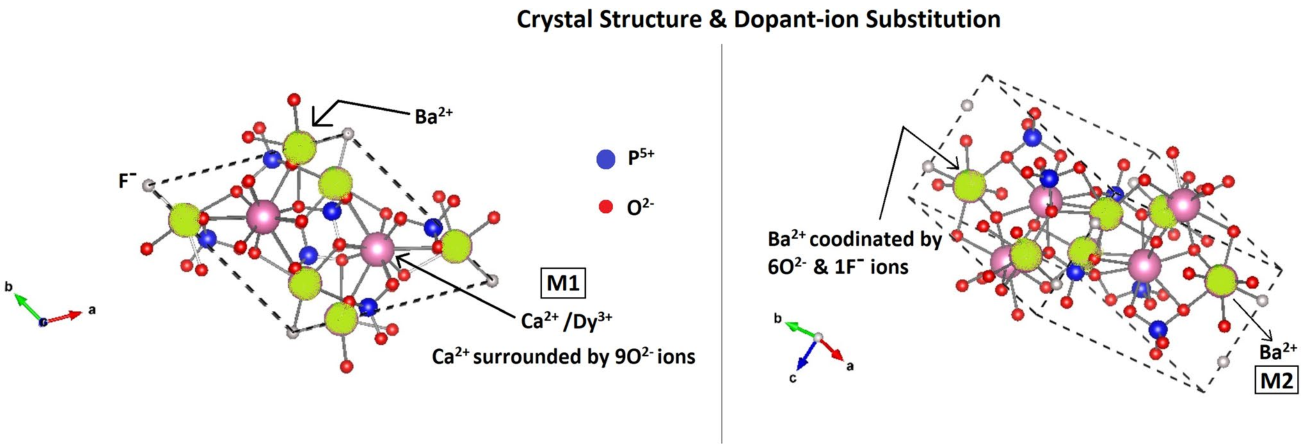

Fig. 6 BCPOF host crystal structure with probable Dy substitution sites.

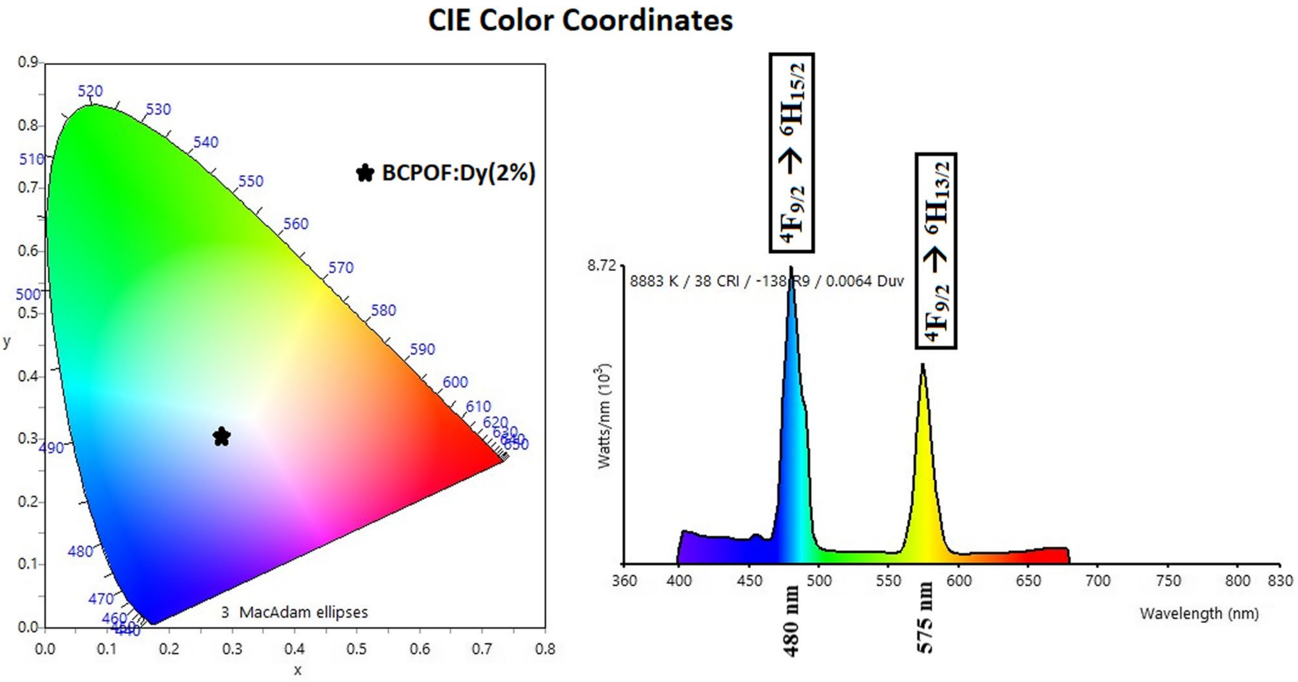

Fig. 7 The Commission Internationale de L'Eclairage (CIE) 1931 chromaticity diagram for the optimized BCPOF:Dy (2%) sample, with PL spectra exhibiting both bluish-yellow emissions (Color figure online).

Table III CIE color chromaticity (1931) parameters

Phosphor	(*x*, *y*)	(*u*′, *v*′)	CCT (K)	Application in w-LEDs (K)	Color purity (CP)	Dominant wavelength (nm)	CRI (Ra)
BCPOF:Dy^{3+} (0.5%)	0.2929, 0.2824	0.2019, 0.4380	8966	> 5000, cool	19.0%	471.4	90
BCPOF:Dy^{3+} (1%)	0.2839, 0.2768	0.1973, 0.4330	10348	> 5000, cool	22.4%	474.1	79
BCPOF:Dy^{3+} (2%)	0.2843, 0.3049	0.1867, 0.4506	8883	> 5000, cool	18.9%	483.9	38
BCPOF:Dy^{3+} (3%)	0.2907, 0.3030	0.1920, 0.4504	8407	> 5000, cool	17.0%	481.9	53
BCPOF:Dy^{3+} (5%)	0.2914, 0.3043	0.1920, 0.4512	8317	> 5000, cool	16.7%	482.2	53
BCPOF:Dy^{3+} (7%)	0.2893, 0.3018	0.1915, 0.4495	8561	> 5000, cool	17.6%	481.8	55

Following McCamy's relation,

$$\mathrm{CCT} = -449n^3 + 3525n^2 - 6823.3n + 5520.33 \tag{5}$$

where $n = (x - x_e)/(y - y_e)$, (x, y) represents the main CIE 1931 chromaticity coordinates, and (x_e, y_e) as (0.332, 0.186) implies the epicenters of the convergence.

$$\text{Color Purity} = \sqrt{\frac{\left(x - x_i\right)^2 + \left(y - y_i\right)^2}{\left(x_d - x_i\right)^2 + \left(y_d - y_i\right)^2}} \times 100\% \tag{6}$$

where (x, y), (x_i, y_i), and (x_d, y_d) denote the CIE coordinates, white light illuminants, and coordinates of the dominant wavelength, respectively, of the proposed phosphor.[50,53,55]

CIE coordinates were essentially observed for the PL emission in the range of 400–680 nm.

Conclusions

$Ba_3Ca_2(PO_4)_3F$ (BCPOF) is a scarcely investigated fluorapatite compound that exists as a mineral in the earth's crust, making it useful and attractive in the view of geological and petrological fields. Efficient green luminescence upon the addition of europium ions was previously reported in this crystal. Therefore, in this work, a new phosphor employing BCPOF as host material with white light inclinations doped with dysprosium was synthesized using a traditional solid-state reaction method.

Detailed x-ray diffraction and Rietveld studies identified the successful formation of the desired composition in our samples. The crystallite sizes calculated using Scherrer's and W–H formulas were found to be comparable and in the nanometer range. Photoluminescence results showed characteristic emission of Dy^{3+} comprising two peaks. Lifetime measurements gave decay time in milliseconds for the recorded curves. The value of the intrinsic radiative lifetime (τ_R) was determined from the experimental data, yielding a unit-less value equal to 0.87. The magnitude of non-radiative decay rates increased consistently with increasing Dy^{3+} concentration within the host lattice, resulting in easy triggering of relaxation processes due to the close proximity of dopant ions. Further, we observed the best CRI for the sample with the lowest amount of Dy doping. The CIE color chromaticity coordinates were estimated by plotting points on the MacAdam ellipse diagram. All the samples with different Dy concentrations were found to produce efficient white light emission on excitation with a 348 nm wavelength. Also, other CIE parameters indicated poor color purity and high CCT (K) values for our samples, in concordance with ideal white light specifications. High CCT (K) could be tuned for use in outdoor lighting applications.

Acknowledgments Author Shruti Dhale is extremely thankful to the Government of Maharashtra, India, for providing research assistance under a Mahajyoti fellowship (2022) for carrying out present work. Author Vartika Singh is also highly indebted to CSIR, Government of India, for providing financial support through Grant No. 31/0001(11936)/2021-EMR-I. The authors are also thankfully indebted to Dr. Naval Kishor Upadhyay of Advanced Carbon Products Metrology Section, CSIR-National Physical Laboratory, New Delhi, for XRD measurements.

Author Contributions SD: Experimental & Investigation, NU: Conceptualization & Methodology, VSS: Formal analysis & Writing—original draft, SRD: Visualization & Supervision, AB: Calculations, RK: Supervision, SVM: Basic concept.

Data Availability Data will be made available on reasonable request.

Conflict of interest No potential conflict of interest was reported by the authors.

Ethical Approval This manuscript does not contain any data which needed ethical approval, and the research does not involve human participants and/or animals.

References

1. M. Kottaisamy, R. Jagannathan, P. Jeyagopal, R.P. Rao, and R. Narayanan, Eu^{2+} luminescence in $M_5(PO_4)_3X$ apatites, where M is Ca^{2+}, Sr^{2+} and Ba^{2+}, and X is F^-, Cl^-, Br^- and OH. *J. Phys. D Appl. Phys.* 27(10), 2210 (1994). https://doi.org/10.1088/0022-3727/27/10/034.
2. K.H. Butler, *Fluorescent Lamp Phosphors* (Penn State University Press, 1986).
3. B.M.J. Smets, Phosphors based on rare-earths, a new era in fluorescent lighting. *Mater. Chem. Phys.* 16(3–4), 283 (1987). https://doi.org/10.1016/0254-0584(87)90103-9.
4. J.-P. Budin, J.-C. Michel, and F. Auzel, Oscillator strengths and laser effect in $Na_2Nd_2Pb_6(PO_4)_6Cl_2$ (chloroapatite), a new high-Nd-concentration laser material. *J. Appl. Phys.* 50, 641 (1979). https://doi.org/10.1063/1.326023.
5. A.G. Werner, Geschichte, Karakteristik, und kurze chemische Untersuchung des Apatits (History, characteristics, and brief chemical investigation of apatite. *Bergmännisches J. Min. J.* 1, 76 (1788).
6. M. Shang, D. Geng, D. Yang, X. Kang, Y. Zhang, and J. Lin, Luminescence and energy transfer properties of $Ca_2Ba_3(PO_4)_3Cl$ and $Ca_2Ba_3(PO_4)_3Cl$: A (A = E^{u2}+/C^{e3}+/D^{y3}+/T^{b3}+) under UV and low voltage electron beam excitation. *Inorg. Chem.* 52, 3102 (2013). https://doi.org/10.1021/ic3025759.
7. X. Chen, P. Dai, X. Zhang, C. Li, S. Lu, X. Wang, Y. Jia, and Y. Liu, A Highly efficient white light (Sr_3, Ca, Ba)($_PO_4$)3Cl:^{Eu}2+, ^{Tb}3+, ^{Mn}2+ phosphor via dual energy transfers for white light-emitting diodes. *Inorg. Chem.* 53, 3441 (2014). https://doi.org/10.1021/ic402870p.
8. D. Nishio-Hamane, Y. Ogoshi, and T. Minakawa, Miyahisaite, (Sr, $Ca_)2B_a3(P_O4_)3F$, a new mineral of the hedyphane group in the apatite supergroup from the Shimoharai mine, Oita Prefecture, Japan. *J. Min. Petrol. Sci.* 107(3), 121 (2012). https://doi.org/10.2465/jmps.110901.
9. Z. Fu, X. Wang, Y. Yang, Z. Wu, D. Duan, and X. Fu, Hydrothermal synthesis, electronic structure and tunable luminescence of single-phase $Ca_5(PO_4)_3F$:Tb^{3+}, E^{u3}+ microrods. *Dalton Trans.* 43, 2819 (2014). https://doi.org/10.1039/C3DT52231H.
10. N. Guo, H. You, Y. Song, M. Yang, K. Liu, Y. Zheng, Y. Huang, and H.J. Zhang, White-light emission from a single-emitting-component $Ca_9Gd(PO_4)_7$:Eu^{2+}, M^{n2}+ phosphor with tunable luminescent properties for near-UV light-emitting diodes. *J. Mater. Chem.* 20, 9061 (2010). https://doi.org/10.1039/C0JM01860K.
11. R. Sahoo, S.K. Bhattacharya, and R. Debnath, A new type of charge compensating mechanism in $Ca_5(PO_4)_3F$:Eu^{3+} phosphor. *J. Solid State Chem.* 175, 218 (2003). https://doi.org/10.1016/S0022-4596(03)00249-4.
12. Q. Zeng, H. Liang, G. Zhang, M.D. Birowosuto, Z. Tian, H. Lin, Y. Fu, P. Dorenbos, and Q. Su, Luminescence of Ce^{3+} activated fluoro-apatites $M_5(PO_4)_3F$(M= Ca, Sr, Ba) under VUV–UV and x-ray excitation. *J. Phys. Condens. Matter* 18, 9549 (2006). https://doi.org/10.1088/0953-8984/18/42/002.
13. G. Blasse, Influence of local charge compensation on site occupation and luminescence of apatites. *J. Solid State Chem.* 14(2), 181 (1975). https://doi.org/10.1016/0022-4596(75)90009-2.
14. R.G. Pappalardo, J. Walsh, and R.B. Hunt Jr., Cerium-activated halophosphate phosphors I. *Strontium Fluoroapatites. J. Electrochem. Soc.* 130, 2087 (1983). https://doi.org/10.1149/1.2119528.
15. M. Gaft, G. Panczer, R. Reisfeld, and E. Uspensky, Laser-induced time-resolved luminescence as a tool for rare-earth element identification in minerals. *Phys. Chem. Miner.* 28, 347 (2001). https://doi.org/10.1007/s002690100163.
16. J. Ding, Q. Wu, Y. Li, Q. Long, C. Wang, and Y. Wang, $Sr_{7.3}Ca_{2.7}(PO_4)_6F_2$: Eu^{2+}, Mn^{2+}: a novel single-phased white light emitting phosphor for NUV-LEDs. *Dalton Trans.* 44, 9630 (2015). https://doi.org/10.1039/C5DT00907C.
17. N. Guo, H. You, C. Jia, R. Ouyang, and D. Wu, A Eu^{2+} and Mn^{2+}-coactivated fluoro-apatite-structure $Ca_6Y_2Na_2(PO_4)_6F_2$ as a standard white-emitting phosphor via energy transfer. *Dalton Trans.* 43, 12373 (2014). https://doi.org/10.1039/C4DT01021C.
18. M. Jiao, Y. Jia, W. Lu, W. Lv, Q. Zhao, B. Shao, and H. You, $Sr_3GdNa(PO_4)_3F$:Eu^{2+}, M^{n2}+: a potential color tunable phosphor

for white LEDs. *J. Mater. Chem. C* 2, 90 (2014). https://doi.org/10.1039/C3TC31837K.

19. K. Li, D. Geng, M. Shang, Y. Zhang, H. Lian, and J. Lin, Color-tunable luminescence and energy transfer properties of Ca$_9$Mg(PO$_4$)$_6$F$_2$:Eu^{2+}, Mn^{2+} phosphors for UV-LEDs. *J. Phys. Chem. C* 118, 11026 (2014). https://doi.org/10.1021/jp501949m.
20. C. Fouassier, B. Latourrette, J. Portier, and P. Hagenmuller, Nature de la fluorescence de l'europium divalent dans les fluorures. *Mat. Res. Bull.* 11, 933 (1976). https://doi.org/10.1016/0025-5408(76)90166-5.
21. W.A. Hargreaves, Energy levels of Pr^{3+} ions in halide crystals. *J. Phys. Condens. Matter* 4, 6141 (1992). https://doi.org/10.1088/0953-8984/4/28/015.
22. C.W. Struck and W.H. Fonger, Unified model of the temperature quenching of narrow-line and broad-band emissions. *J. Lumin.* 10, 1 (1975). https://doi.org/10.1016/0022-2313(75)90029-0.
23. K.C. Bleijenberg and G. Blasse, QMSCC calculations on thermal quenching of model phosphor systems. *J. Solid State Chem.* 28, 303 (1979). https://doi.org/10.1016/0022-4596(79)90081-1.
24. C. Zeng, Y. Hu, Z. Xia, and H. Huang, A novel apatite-based warm white emitting phosphor Ba$_3$GdK(PO$_4$)$_3$F:Tb^{3+}, E^{u3}+ with efficient energy transfer for w-LEDs. *RSC Adv.* 5, 68099 (2015). https://doi.org/10.1039/C5RA11844A.
25. X. Meng, K. Qiu, Z. Tian, X. Shi, J. You, Z. Wang, P. Li, and Z. Yang, Tunable-emission single-phase phosphors Ba$_3$Ca$_2$(PO$_4$)$_3$F: M (M=C^{e3}+, E^{u2}+, Mn^{2+}): Crystal structure, luminescence and energy transfer. *J. Alloys Compd.* 719, 322 (2017). https://doi.org/10.1016/j.jallcom.2017.05.197.
26. M. Zheng, Z. Wang, X. Wang, J. Cui, Y. Yao, M. Zhang, Z. Yang, L. Cao, and P. Li, Recent progress of effect of crystal structure on luminescence properties of Ce^{3+}–Eu^{2+} Co-doped phosphors. *RSC Adv.* 11, 26354 (2021). https://doi.org/10.1039/D1RA04700K.
27. Yu.V. Shchapova, S.L. Votyakov, G.B. Mikhalevsky, VYu. Ivanov, and V.A. Pustovarov, Impurity luminescence centers in fluorapatite from quartz-bearing paragenesis according to photo- cathode- and synchrotron-induced luminescence. *Geodyn. Tectonophys.* 13(2s), 1–9 (2022). https://doi.org/10.5800/GT-2022-13-2s-0610.
28. Y. Lv, Z. Li, Y. Jin, H. Wu, C. Wang, G. Ju, L. Chen, Z. Hu, and Y. Hu, A novel photochromic material based on halophosphate: Remote lightcontrolled reversible luminescence modulation and fluorescence lifetime regulation. *Ceram. Int.* 45, 5971 (2019). https://doi.org/10.1016/j.ceramint.2018.12.067.
29. P. Kaur, S. Rani, and A.K. Srivastava, Luminescence study of Dy^{3+} doped magnesium aluminate phosphors for white light. *Z. Anorg. Allg. Chem.* 649(13), e202300015 (2023). https://doi.org/10.1002/zaac.202300015.
30. Y.-G. Yang, X.-P. Wang, B. Liu, Y.-Y. Zhang, X.-S. Lv, J. Li, L. Wei, H.-J. Yu, Y. Hu, and H.-D. Zhang, Molten salt synthesis and luminescence of Dy^{3+}-doped Y$_3$Al$_5$O$_{12}$ phosphors. *Luminescence* 35(4), 580 (2020). https://doi.org/10.1002/bio.3759.
31. S. Chemingui, M. Ferhi, K. Horchani-Naifer, and M. Férid, Synthesis and luminescence characteristics of Dy^{3+} doped KLa(PO$_3$)$_4$. *J. Lumin.* 166, 82 (2015). https://doi.org/10.1016/j.jlumin.2015.05.018.
32. K. Linganna, Ch.S. Rao, and C.K. Jayasankar, Optical properties and generation of white light in Dy^{3+}-doped lead phosphate glasses. *J. Quant. Spectrosc. Radiat. Transf.* 118, 40–48 (2013). https://doi.org/10.1016/j.jqsrt.2012.12.002.
33. S. Slimi, E. Madirov, A. Turshatov, B.S. Richards, R. Maria Sole, M. Aguilo, F. Dıaz, E.B. Salem, and X. Mateos, Structure and luminescence properties of Dy^{3+} doped quaternary tungstate Li$_3$Ba$_2$Gd$_3$(WO$_4$)$_8$ for application in wLEDs. *RSC Adv.* 13, 23772 (2023). https://doi.org/10.1039/D3RA02501B.
34. E. Kolesnikov, A.A. Kalinichev, M.A. Kurochkin, E.V. Golyeva, A.S. Terentyeva, EYu. Kolesnikov, and E. Lähderanta, Structural, luminescence and thermometric properties of nanocrystalline YVO$_4$:Dy^{3+} temperature and concentration series. *Sci. Rep.* 9, 2043 (2019). https://doi.org/10.1038/s41598-019-38774-6.
35. N. Jaidass, C.K. Moorthi, A.M. Babu, and M.R. Babu, Luminescence properties of Dy^{3+} doped lithium zinc borosilicate glasses for photonic applications. *Heliyon* 4(3), e00555 (2018). https://doi.org/10.1016/j.heliyon.2018.e00555.
36. J. Zhang, Q. Guo, L. Liao, Y. Wang, M. He, H. Ye, L. Mei, H. Liu, and T. Zhou, and Bin Ma, Structure and luminescence properties of La$_6$Ba$_4$(SiO$_4$)$_6$F$_2$:Dy^{3+} phosphor with apatite structure. *RSC Adv.* 8, 38883 (2018). https://doi.org/10.1039/C8RA08324J.
37. K. Griebenow, M.-P. Truong, F. Munoz, and R. Klement, and Dusan Galusek, Tuning the fluorescence of Dy^{3+} via the structure of borophosphate glasses. *Sci. Rep.* 13, 1919 (2023). https://doi.org/10.1038/s41598-023-28941-1.
38. R.B. Deepali, H.K. Vandana, and M. Jayasimhadri, Structural and spectroscopic properties of Sm^{3+}-doped NaBaB$_9$O$_{15}$ phosphor for optoelectronic device applications. *J. Mater. Sci. Mater. Electron.* 32, 1650 (2021). https://doi.org/10.1007/s10854-020-04934-y.
39. M. Dahiya, A. Siwach, M. Dalal, and D. Kumar, Study of structural and luminescent characteristics of novel color tunable blue-green Tb^{3+}-doped Na$_3$Y(PO$_4$)$_2$ nanoparticles for NUV-based WLEDs. *J. Mater. Sci. Mater. Electron.* 32, 4166 (2021). https://doi.org/10.1007/s10854-020-05158-w.
40. D.K.S. Kumar and J. Manam, Structural and optical properties of highly thermally active Gd2Zr2O7:Dy3+ phosphors for lighting applications. *J. Mater. Sci. Mater. Electron.* 30, 2360 (2019). https://doi.org/10.1007/s10854-018-0509-8.
41. M. Sukumar, M. Agila, A. Sutha, V. Ravi, A.M. Al-Enizi, M. Ubaidullah, M.S. Samdani, M. Sundararajan, and B. Pandit, Temperature-dependent phase transition: structural, optical, magnetic and dielectric properties of La$_2$CuO$_4$ perovskite nanoparticles. *J. Mater. Sci. Mater. Electron.* 33, 26144 (2022). https://doi.org/10.1007/s10854-022-09301-7.
42. P. Chhillar, M. Bedi, A. Hooda, M. Punia, V.B. Taxak, S.P. Khatkar, and P.B. Doon, Synthesis and optoelectronic features of cool white light-emitting Ba$_3$GdP$_3$O$_{12}$: Dy^{3+} nanophosphors for multifarious application prospects. *J. Mater. Sci. Mater. Electron.* 33, 26343 (2022). https://doi.org/10.1007/s10854-022-09316-0.
43. C.-W. Huang, B.-J. Lin, H.-Y. Lin, C.-H. Huang, F.-Y. Shih, W.-H. Wang, C.-Y. Liu, and H.C. Chui, *Nanoscale Res. Lett.* 8(1), 480 (2013). https://doi.org/10.1186/1556-276X-8-480.
44. V. Ganesh and I.S. Yahia, Cerium-doped Bi$_2$S$_3$ thin films fabricated by nebulizer-assisted spray pyrolysis method for photodetector applications. *J. Electron. Mater.* 52, 5901 (2023). https://doi.org/10.1007/s11664-023-10482-y.
45. K. Ou, S. Wang, L. Bai, Y. Wang, K. Zhang, and L. Yi, Investigation on annealing temperature-dependent optical properties of electron beam evaporated ZnSe thin films. *Thin Solid Films* 669, 247 (2019). https://doi.org/10.1016/j.tsf.2018.11.013.
46. K. Paulraj, S. Ramaswamy, N. Chidhambaram, H. Algarni, M. Shkir, and S. AlFaify, Investigation of samarium-doped PbS thin films fabricated using nebulizer spray technique for photosensing applications. *Superlattices Microstruct.* 148, 106723 (2020). https://doi.org/10.1016/j.spmi.2020.106723.
47. H. Demir, Ö. Şahin, O. Baytar, and S. Horoz, Investigation of the properties of photocatalytically active Cu-doped Bi$_2$S$_3$ nanocomposite catalysts. *J. Mater. Sci. Mater. Electron.* 31, 10347 (2020). https://doi.org/10.1007/s10854-020-03582-6.
48. S. Sharma, P. Kumar, M. Kumar, V. Singh, R.I. Yocupicio-Gaxiola, J.M. Siqueiros, and O.R. Herrera, Investigations on dielectric, transport, and ferroelectric properties of Ca-modified Bi$_{0.80}$La$_{0.20}$FeO$_3$ ceramic synthesized by solid state reaction route. *J. Electron. Mater.* 52, 4312 (2023). https://doi.org/10.1007/s11664-023-10209-z.
49. Q. Su, Z. Pei, L. Chi, H. Zhang, and Z. Zhang, and Feng Zou, The yellow-to-blue intensity ratio (Y/B) of Dy^{3+} emission. *J. Alloys*

Compd. 192, 25 (1993). https://doi.org/10.1016/0925-8388(93)90174-L.

50. R. Shrivastava, J. Kaur, and V. Dubey, White light emission by Dy^{3+} doped phosphor matrices: a short review. *J. Fluoresc.* 26, 105 (2016). https://doi.org/10.1007/s10895-015-1689-8.
51. L. Reddy, A review of the efficiency of white light (or other) emissions in singly and co-doped Dy^{3+} ions in different host (phosphate, silicate, aluminate) materials. *J. Fluoresc.* 33, 2181 (2023). https://doi.org/10.1007/s10895-023-03250-y.
52. Z.T. Naik, P. Ankoji, and B.H. Rudramadevi, Luminescence properties of dysprosium doped fluoroborate optical glasses. *Spectrosc. Lett.* 55(4), 250 (2022). https://doi.org/10.1080/00387010.2022.2056614.
53. V.S. Singh, S.R. Dhakate, P.V. Tumram, P.D. Belsare, and S.V. Moharil, Probing into photoluminescence properties of trivalent rare earths (Gd^{3+}/Tb^{3+}/Dy^{3+}/Eu^{3+}) activated fluoro-elpasolites. *J. Mater. Sci. Mater. Electron.* 34, 1087 (2023). https://doi.org/10.1007/s10854-023-10506-7.
54. V.S. Singh, S.R. Dhakate, P.D. Belsare, R. Nafdey, and S.V. Moharil, Investigating photoluminescence in Gd^{3+} activated pyrochlore-type fluoro-aluminates. *Radiat. Eff. Defects Solids* 178(9–10), 1159 (2023). https://doi.org/10.1080/10420150.2023.2234066.
55. C.S. McCamy, Correlated color temperature as an explicit function of chromaticity coordinates. *Color. Res. Appl.* 17, 142–144 (1992). https://doi.org/10.1002/col.5080170211.